Author(s): Werbrouck, Andreas; Mattelaer, Felix; Minjauw, Matthias; Nisula, Mikko; Julin, Jaakko; Munnik, Frans; Dendooven, Jolien; Detavernier, Christophe

Title: Reaction Pathways for Atomic Layer Deposition with Lithium Hexamethyl Disilazide, Trimethyl Phosphate, and Oxygen Plasma

Year: 2020

Version: Accepted version (Final draft)

Please cite the original version:

Werbrouck, A., Mattelaer, F., Minjauw, M., Nisula, M., Julin, J., Munnik, F., Dendooven, J., & Detavernier, C. (2020). Reaction Pathways for Atomic Layer Deposition with Lithium Hexamethyl Disilazide, Trimethyl Phosphate, and Oxygen Plasma. Journal of Physical Chemistry C, 124(50), 27829-27839. https://doi.org/10.1021/acs.jpcc.0c09284

Reaction Pathways for Atomic Layer Deposition with Lithium Hexamethyl Disilazide, Trimethyl Phosphate and Oxygen Plasma

Andreas Werbrouck,[†] Felix Mattelaer,[†] Matthias Minjauw,[†] Mikko Nisula,[†] Jaakko Julin,[‡] Frans Munnik,[¶] Jolien Dendooven,[†] and Christophe Detavernier*,[†]

[†]*Ghent University, Department of Solid State Sciences, Krijgslaan 281, 9000 Ghent, Belgium*

[‡]*University of Jyväskylä, Department of Physics, P.O. Box 35, 40014 Jyväskylä, Finland*

[¶]*Helmholtz-Zentrum Dresden-Rossendorf, Institute of Ion Beam Physics and Materials Research, Bautzner Landstraße 400, 01328 Dresden, Germany*

E-mail: Christophe.Detavernier@ugent.be

Abstract

Atomic layer deposition (ALD) of lithium-containing films is of interest for the development of next-generation energy storage devices. Lithium hexamethyl disilazide (LiHMDS) is an established precursor to grow this type of films. The LiHMDS molecule can either be used as a single-source precursor molecule for lithium, or as a dual-source precursor molecule for lithium and silicon. Single-source behaviour of LiHMDS is observed in the deposition process with trimethylphosphate (TMP) resulting in the deposition of crystalline lithium phosphate (Li_3PO_4). In contrast, LiHMDS exhibits dual-source behavior when combined with O_2 plasma, resulting in a lithium silicate. Both processes were characterized with in situ ellipsometry, in situ time-resolved full-range mass spectrometry, x-ray photoelectron spectroscopy (XPS) and elastic recoil detection analysis (ERDA). When we combined both reactants into a three-step LiHMDS-TMP-O_2* or LiHMDS-O_2*-TMP process, the dual-source nature of LiHMDS emerged again. By carefully combining our measurements, it is shown that film growth with LiHMDS (in combination with TMP and O_2 plasma) is driven by dipole-driven self-saturated surface interactions combined with dissociative chemisorption. We show that when hydroxyl groups are present on the surface, silicon will be incorporated in the films. These insights benefit the general understanding of the behaviour of the LiHMDS and TMP precursors, and may facilitate their effective use in ternary or quaternary processes.

Introduction

For the development of next-generation lithium-ion batteries, the ability to tailor interfaces at the atomic scale will be of importance, given the role interfacial reactions play in the chemical processes governing the operation and the degradation of batteries. Atomic layer deposition (ALD), a gas-phase deposition technique based on sequential, self-limiting pulses of precursor molecules, enables modification of these interfaces by coating them with a thin film.[1,2] Though ALD films have found their application as interfacial coatings,[3,4] and as electrodes for 3D thin film batteries,[1,5–8] the direct deposition of lithium-containing compounds may further enhance the interface

quality and battery performance. Deposition of lithium-containing electrodes could be beneficial to avoid post-lithiation steps. In addition, ALD of Li-containing thin films opens the way to conformal deposition of solid-state electrolytes for 3D thin film batteries.[9–13]

Several precursors have been used up to now to deposit lithium-containing films, of which LiO^tBu (lithium tert-butoxide) is by far the most popular one. However, LiHMDS (lithium hexamethyl disilazide, or lithiumbis(trimethylsilyl)amide) may be more convenient for some applications due to its lower cost, and the lower source temperature at which it can be vaporized. Furthermore, in LiHMDS the lithium atom is bound to a nitrogen atom, which makes it easier to deposit oxygen-free films, or to control the source of oxygen in the films more precisely. However, due to the presence of the silyl groups in the LiHMDS molecule, silicon can be built into the film, either on purpose or as a contaminant. This makes it important to untangle the mechanisms leading to either single-or dual-source behaviour.

Lithium silicate can be grown with LiHMDS and ozone, as reported by Hämäläinen *et al.*[14] with a growth rate of about 0.8 Å/cycle at 250°C. The growth per cycle increased with temperature from 150°C up to 400°C. The Li content of the films was consistently about 30%, but the Si content increased with temperature from 11.2% to 18.5%, while the C content decreased from 3.94% to 0.15% and O content increased from 44.2% at 150°C to 49.6% at 350°C. This could point to growth of a lithium carbonate component at lower temperatures. At 400°C the onset of LiHMDS decomposition was likely observed. Tomczak *et al.* have investigated this process with in situ mass spectrometry, infrared spectrometry and DFT calculations.[15] From these measurements, it was concluded that during the adsorption of LiHMDS on a hydroxylated surface, HMDS is formed as a reaction product. The HMDS then also reacts with available hydroxyl groups, leading to silicon incorporation in the film. Hence the dual-source behaviour of LiHMDS with ozone was explained by the *in situ* generation of HMDS, which is a known precursor for Si.[16] A similar observation was made by Miikkulainen *et al.*[17] when trying to use LiHMDS in a 4-step process with H_2O and O_3, which resulted in uncontrolled growth and non-uniform films. From the calculations in ref.,[15] it was clear that compared to HMDS, LiHMDS has a large dipole moment. This suggests that

physisorption may as well play an important role in the reaction mechanism.

Hämäläinen *et al.* reported on the growth of crystalline lithium phosphate (Li_3PO_4), combining LiO^tBu or LiHMDS with trimethylphosphate (TMP).[18] With the LiHMDS, again a constantly increasing growth per cycle was observed for increasing substrate temperature between 275°C and 350°C, with a growth of about 0.5 Å/ cycle at 300°C, and very little growth below 275°C. One of the most fascinating properties of this process is that it does not need an additional source of oxygen, in contrast to other phosphate processes, where TMP is used in combination with H_2O, oxygen (plasma) and ozone.[10,19–21] In itself, the addition of an oxygen source is rather counter-intuitive, since oxygen is already present in TMP. It is also interesting to note that generic processes of the form TMP-oxygen source do not seem to yield any film. Only when it is part of a subcycle in a 3-or 4-step processes, some phosphates can be grown.[8,20,22] This suggests that the function of the oxygen/ozone/water in these processes is to remove remaining methyl groups and rehydroxylate the surface, opening up reaction pathways for another precursor. In contrast with these 3-step processes no additional step is necessary for the reaction of TMP with LiHMDS to take place.

Recently, within our group a new way of conducting *in situ* mass spectrometry was developed.[23] One way of conducting regular mass spectrometry experiments is to track, with a proper time resolution, the intensity of a few specific masses that are deemed relevant. This way, it is always possible to overlook other relevant masses. Another way of measuring is to probe a full m/z-range (for example m/z 10-200). This takes a lot of time: obtaining full spectra like this is time consuming and therefore does not allow measuring transient signals during an ALD process. The hybrid strategy we first proposed in[23] is able to obtain time-resolved, full-range m/z spectra. This is achieved by scanning all masses with a relatively poor time resolution, but repeating this during a large number of subsequent ALD cycles. Using the exact timestamp of each datapoint (m/z, time, intensity), one can then calculate back when exactly in the ALD cycle it was measured, and thus construct a complete and detailed time-resolved m/z spectrum of a full ALD cycle. These spectra are visualized by means of a heat map graph (for an example, see figure 2) of which slices can be shown. In this paper, we use this mass spectrometry method in conjunction with composition and

thickness measurements to investigate the single-source and dual-source behaviour of LiHMDS in relation to TMP, O_2 plasma and combinations thereof.

In the course of this work, we will show that LiHMDS reacts differently depending on the surface. Hydroxyl groups will lead to dissociation of the molecule, as described by Tomczak *et al.*[15] However dipole-driven physisorption with surface O-Li groups is another mechanism that can lead to the adsorption of the entire LiHMDS molecule. The next precursor step then determines whether lithium alone, or lithium and silicon are incorporated.

Methods

All depositions and experiments were carried out in a home-built, pump-type ALD reactor, equipped with an inductively coupled RF (13.56 MHz) plasma. The walls were heated to 130°C, LiHMDS (Sigma-Aldrich, 97%) was heated to 90°C, TMP (Sigma-Aldrich, 97%) to 45°C. The plasma power used for all depositions was 300W.

Ellipsometry (J.A. Woollam F2000 ellipsometer) was available both in situ via optical viewports and ex situ via a manual stage. Time-resolved mass spectrometry was conducted as described in ref.[23] with about 1 g Al_2O_3 powder (3 μm grain size) in the reactor to increase the amount of reactive surface and the amount of generated reaction products. Assuming spherical particles, this leads to a lower bound of 0.5 m^2 active surface area. The regular AB cycle is, for the sake of internal reference, turned into a repeated (AAA)B cycle: precursor A is pulsed 3 times subsequently. The brackets denote the measurements of the mass spectrometer: during the pulse of precursor B, access to the spectrometer is prevented to minimize coating of the interior of the spectrometer. After this an A(BBB) process is characterized. The three-step ABC processes were characterized in a similar fashion. Each cycle regime was repeated 30 times. The m/z was scanned from 10 to 200 amu, with a dwell time of 20 ms, resulting in a scan time of 3.82 s. After reorganizing the data a rolling average with a box-size of 10 was used on every m/z to smoothen the data.

Thick samples have been analysed with ERDA (Elastic Recoil Detection Analysis) using a 43

MeV Cl^{7+} ion beam. The angle between the sample normal and the incoming beam is 75°, the scattering angle is 30°. The analysed area is about 2 × 2 mm. The recoil atoms and scattered ions have been detected with a Bragg Ionisation Chamber (BIC), which enables energy measurement and Z identification of the particles. H and Li recoils have been detected with a separate solid state detector at a scattering angle of 40°. This detector is preceded by a 25 μm Kapton foil to stop scattered ions and heavy recoil ions. The depth resolution of this system is reduced because of energy loss straggling in the foil. Both elements are well separated in the spectra.

X-ray photoelectron spectroscopy (XPS) measurements were performed on a Theta Probe system of Thermo Scientific, operating at a base pressure of $\sim 10^{-10}$ mbar with an Al Kα X-ray excitation source and a 2D channel plate detector. The intensities over different exit angles were integrated. All samples were completely sputtered through, down to the SiO_2 substrate. Ar ions with an energy of 0.5 keV were used for sputtering. An ion current of 700 nA over a sputtering surface of 3×3 mm was used, leading to a low sputter rate. Samples were stored under Ar and only briefly exposed to air prior to XPS and ERDA measurements.

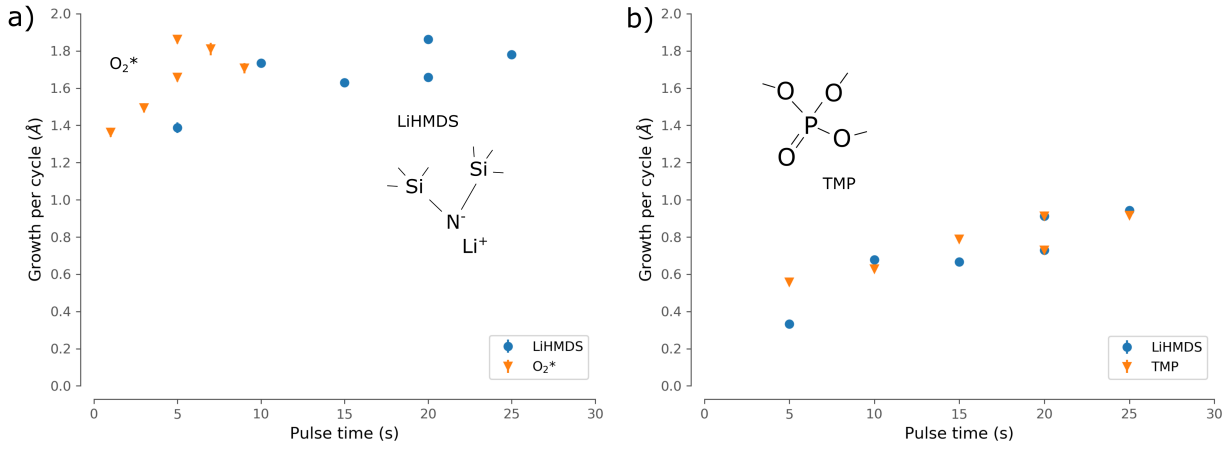

Figure 1: Saturation graphs for a) LiHMDS-O_2* (150°C substrate temperature) and b) LiHMDS-TMP (325°C substrate temperature) processes. During the variation of the O_2* and TMP pulse, the LiHMDS pulse time was kept at 20s. During LiHMDS characterization, the O_2* pulse time was kept at 5 s and the TMP pulse time at 20s. Insets: structures of the precursor molecules used.

Results

Growth characteristics of the studied processes

First, we look into two basic two-step processes with LiHMDS: a first one where LiHMDS is combined with oxygen plasma, very similar to the earlier experiments with ozone,[14] and a second one where LiHMDS is combined with TMP, identical to the process developed by Hämäläinen *et al.*[18]

For the plasma-assisted process, saturation is observed, although the growth per cycle is higher than the growth with ozone (compare Fig.1a with a reported growth of 0.3 Å/cycle at 150 °C and 0.8 Å/cycle at 250 °C[14]). For the thermal process with TMP (Fig.1b) the saturation is less indisputable, but the growth per cycle and temperature window are similar to the values reported by Hämäläinen,[18] and as will be discussed below, mass spectrometry measurements further support the hypothesis that this process exhibits self-saturating characteristics.

In a second series of experiments, the two-step processes were intermixed in an ABC and ACB fashion, covering the different reactant order permutations. Films were deposited for the following cycle sequences: LiHMDS-O_2*, LiHMDS-TMP, LiHMDS-O_2*-TMP and LiHMDS-TMP-O_2*. 600 cycles were used for the LiHMDS-TMP film, 500 cycles for the other depositions.

Thicknesses of the films were measured with spectroscopic ellipsometry (fitted thicknesses are listed in Table 1, optical parameters are listed for completeness in the supplementary table 1). The LiHMDS-TMP thickness is in line with what is expected from the growth curve (Fig. 1), while LiHMDS-O_2* thickness is a bit higher than expected at 150°C i.e. the GPC calculated by dividing the film thickness by the number of applied ALD cycles (600) is higher than the GPC value obtained from the saturation experiment in Fig. 1 (based on 30 cycles per regime). The LiHMDS-TMP-O_2* process exhibited lower growth compared to the other plasma-enhanced processes, while the LiHMDS-O_2*-TMP process exhibited slightly higher growth than the two-step thermal process.

Table 1: Thicknesses and ERDA data for 500/600-cycle films. No traces of N were observed in the ERDA spectra. We do not expect the moderate deviation of 25 °C between the LiHMDS-TMP deposition and the other depositions to influence the results.

Process	T	cycles	nm	GPC (nm)	at/cm^2	Si (%)	O (%)	Li (%)	H (%)	P (%)	C (%)	N (%)
LiHMDS-O_2*	150°C	500	116.18	0.23	1200	23.0	53.9	22.6	0.5	-	-	-
LiHMDS-O_2*	300°C	500	122.24	0.24	1017	24.2	54.7	20.4	0.7	-	-	-
LiHMDS-O_2*-TMP	300°C	500	134.33	0.27	1111	22.0	58.5	17.3	0.2	2.1	-	-
LiHMDS-TMP-O_2*	300°C	500	78.60	0.16	670	19.2	58.4	18.2	0.5	3.7	-	-
LiHMDS-TMP	325°C	600	49.90	0.08	416	1.2	47.8	28.8	7.1	10.8	4.2	-

Composition of the studied films

The composition of the films was gauged with XPS (Fig. S2) and ERDA (Table 1). The LiHMDS-TMP process deposits, as expected, nearly stoichiometric Li_3PO_4 with some excess O, and H, C and Si contamination.[18] From the composition, it is likely that PO_4 groups from TMP are incorporated as a whole in the film. For the LiHMDS-O_2* silicate films, the Li/Si ratio is not the same as that in the LiHMDS precursor (Li/Si = 0.5), but interestingly it remains close to 1, as opposed to 2.8 (at 150°C) and 1.7 (at 300°C) in the LiHMDS-O_3 process reported by Hämäläinen.[14] The use of O_2* seems to promote silicon incorporation in the films as compared to ozone. In films grown with ternary processes on the other hand, the concentration of P is low but significant: as it is likely that P stays in the PO_4 coordination from the precursor, it is good to realize that (in the case of LiHMDS-TMP-O_2*) 3.7% P accounts for 14.8% O, so 18.5% of the atoms in this film may stem from the TMP molecule. The plasma-assisted processes show no carbon contamination. The hydrogen content may be due to the uptake of water from combustion reactions in the film. This water can then play a role in the so-called reservoir effect which can be a factor to consider for ALD of alkali metals.[1,24,25]

An increase in lithium concentration with increasing depth is visible in the XPS measurements (Fig. S2). ERDA profiles have less depth sensitivity (as opposed to their better accuracy with regards to composition). However, the increased levels of Li at higher depths suggest some kind of sputtering effect when the depth profile is measured. We believe the variation in lithium content with thickness is not an intrinsic characteristic of the films.

The thickness and composition measurements reveal that something interesting is going on in

the ternary processes. The presence of oxygen plasma seems to promote silicon incorporation, hence dual-source behaviour. The composition of films with LiHMDS-O_2* and LiHMDS-O_2*-TMP is very similar. On the other hand, the difference in growth per cycle between LiHMDS-TMP-O_2* and LiHMDS-O_2*-TMP indicates that the order of pulses in the ternary process is important. To further study the reaction mechanism, the four processes were characterized with in situ mass spectrometry (Figs. 2, 3, 4 and 5).

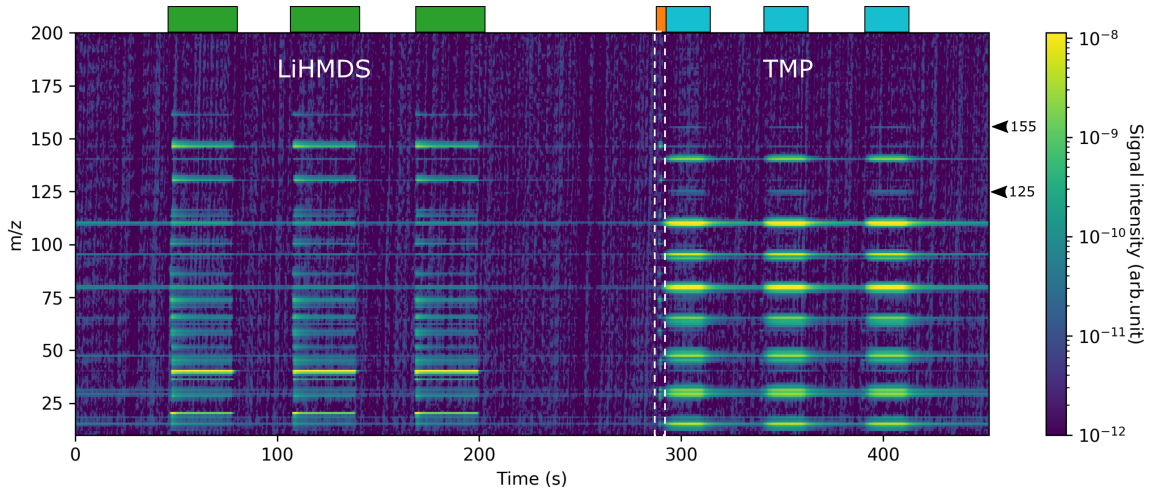

Figure 2: Time-resolved mass spectrum for the LiHMDS-TMP process at 325°C. Reaction products can be observed around $t = 290$s (see dashed box). In the TMP spectrum the peaks at m/z 125 and 155 are anomalous and might as well be (secondary) reaction products. The time-averaged spectrum in the box is shown in Fig. 7. The boxes on top of the figure serve to guide the eye and indicate the assignment of the spectrum to specific molecules (as identified in Table 2). Hence TMP is pulsed from 290 s on, but (CH_3HMDS) is detected as a reaction product (orange box) before we can assign the observed spectrum to TMP (cyan boxes).

Mass spectrometry during LiHMDS-TMP

Mass spectra were gathered following the steps described in ref.,[23] with 1g Al_2O_3 powder (3 μm grain size) at a temperature of 325°C (Fig. 2). To compare, a reference spectrum was collected without powder, with the sample stage at 150°C (Fig. S2). This effectively yields a 'no reaction' fingerprint of the same precursors as the sample temperature is below the threshold for growth. The main difference between Fig. 2 and the no reaction reference in Fig. S2 is the clear presence

Table 2: Peak identification of fragments of complex molecules entering the mass spectrometer in figs. 2, 3, 4 and 5. A molecule does not lose mass when it gets ionized. However, it may not be stable and fall apart into several smaller fragments. When an ionized fragment captures a proton, it may be more stable. This explains excess masses of 1 a.m.u. over the theoretical fragments. In the reverse direction, sometimes smaller masses may be explained by the loss of H atoms from a methyl group. Individual spectra for LiHMDS, TMP and CH_3HMDS are shown in Fig. 7. Several possibilities and explanations for the appearance of some m/z ratios are possible.

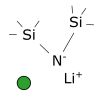

m/z	Fragments/Species
15	CH_3
20	Ar^{+2}
28	Si
36	?
39-40	Ar^+
45	H_2SiCH_3
57	$NSiCH_3$
57−59	$HSi(CH_3)_2$
70	NSi_2
72	$NSi(CH_3)_2$
73	$Si(CH_3)_3$
86	$HNSi_2(CH_3)$
	$NSi(CH_3)_3$
100	$NSi_2(CH_3)_2$
115-118	$NSi_2(CH_3)_3$
130	$NSi_2(CH_3)_4$
145-148	$NSi_2(CH_3)_5$
161	$H-N(Si(CH_3)_3)_2$ (HMDS)

m/z	Fragments
15	CH_3
28-31	OCH_3
47	PO
65	H_2PO_2
79	PO_3
80	HPO_3
95	PO_4
109	$PO_3(CH_3)_2$
110	$(PO_4)(CH_3)$
125	$(PO_4)(CH_3)_2$
140	$(PO_4)(CH_3)_3$

m/z	Fragments
15	CH_3
26-31	NCH_3
45	H_2SiCH_3
51	?
59	$HSi(CH_3)_2$
65-66	?
73-74	$HSi(CH_3)_3$
	$H_2NSi(CH_3)_2$
86	$HNSi(CH_3)Si$
87	$NSi(CH_3)_3$
100	$NSi_2(CH_3)_2$
115	$NSi_2(CH_3)_3$ (observed 113)
130-132	$NSi_2(CH_3)_4$
146-148	$NSi_2(CH_3)_5$
160	$NSi_2(CH_3)_5CH_3$
161	$HN(Si(CH_3)_3)_2$
175	$N(Si(CH_3)_3)_2CH_3$ (CH_3HMDS)

m/z	Species
12	C
16	O
18	H_2O
28	CO
32	O_2
34	$^{17}O_2$
44	CO_2
48	O_3

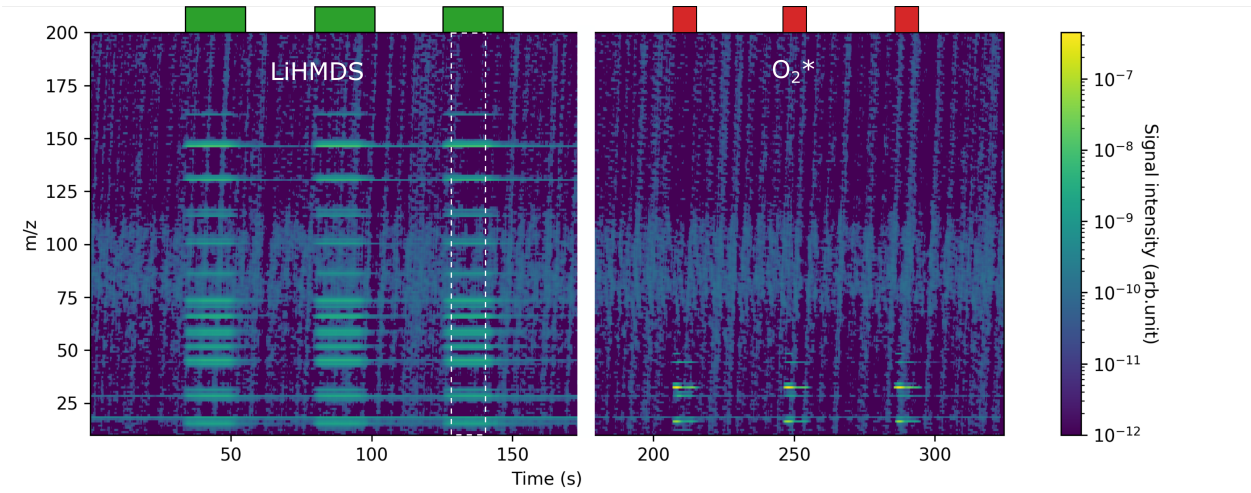

Figure 3: Time-resolved mass spectrum for the LiHMDS-O_2* process at 300°C. The time-averaged spectrum in the box is shown in Fig. 7 as a reference for LiHMDS. Time-resolved spectra for species of interest during the plasma pulse are shown in Fig. 6. The identification of the peaks can be found in Table 2.

of a HMDS-ligand spectrum around 290 s in the beginning of the TMP pulse, right before the TMP spectrum itself becomes visible (see the dashed line box in Fig. 2). The time-averaged mass spectrum for this reaction product is shown in Fig. 7 (3rd row), together with a LiHMDS reference spectrum (1st row). Peak identification for this spectrum can be found in the third column of Table 2. The peaks of this spectrum are attributed to lower mass fragments of CH_3HMDS. On the other hand, no clearly identifiable reaction products can be observed at the beginning of the LiHMDS pulse.

In addition to that, we would like to direct the attention to several other interesting features in the spectra. Because of the ionisation in the mass spectrometer, we see no sign of the full LiHMDS molecule at m/z=167: after ionisation, the molecule quickly loses its lithium atom, and likely captures a proton. This is a known effect in mass spectrometry, but it fully obscures the detection of any HMDS as a reaction product during the LiHMDS pulse. It means that we cannot discern between LiHMDS and its likely reaction product. In the LiHMDS spectrum almost all peaks from the TMP spectrum also emerge. Furthermore, just before the TMP spectrum appears in its second and the third pulse, we still see peaks at m/z 45, 59 and 74 (at 340 s, see figure S3).

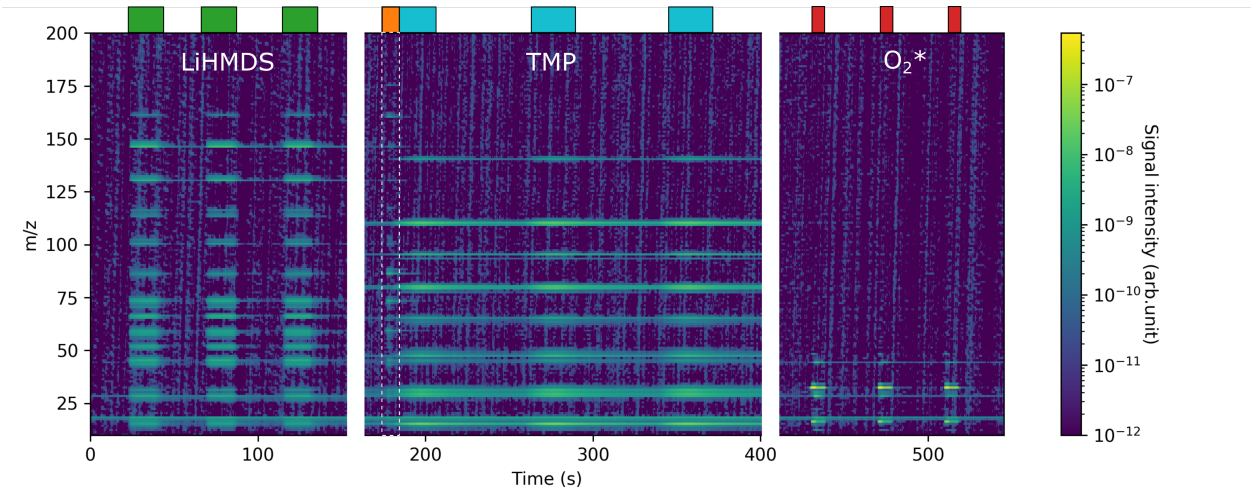

Figure 4: Time-resolved mass spectrum for the LiHMDS-TMP-O_2* process at 300°C. The time-averaged spectrum in the box is shown in Fig. 7. Time-resolved spectra for species of interest during the plasma pulse are shown in Fig. 6. The identification of the peaks can be found in Table 2.

This indicates that the reaction products are formed mainly at the beginning of the pulse. Finally in the TMP spectra in Fig. 2 we clearly see peaks at m/z 125 and 155. These peaks are not present in the reference spectrum. The mass 155 could indicate the presence of $(P(OCH_3)_4)\cdot$.

Mass spectrometry during LiHMDS-O_2*

Time-resolved full-range measurements of the LiHMDS-O_2* process are presented in Fig. 3. It is not possible to obtain a no-reaction reference, as plasma-containing processes will result in growth at lower sample temperatures as well. Note that the maximum of the color scale is about an order of magnitude higher than in Fig. 2 due to the high partial pressure of the oxygen. In the LiHMDS pulse, again no reaction products are observed, possibly due to a strong overlap between precursor and reaction product fragments. The time averaged spectrum recorded during the 3rd LiHDMS pulse (indicated by the box in Fig. 3) is used as a reference spectrum for LiHDMS shown in Fig. 7a and listed in Table 2.

In the oxygen pulse, typical combustion reaction products are observed. Horizontal slices of spectra during the oxygen plasma pulse are shown in Fig. 6a. We can clearly distinguish between

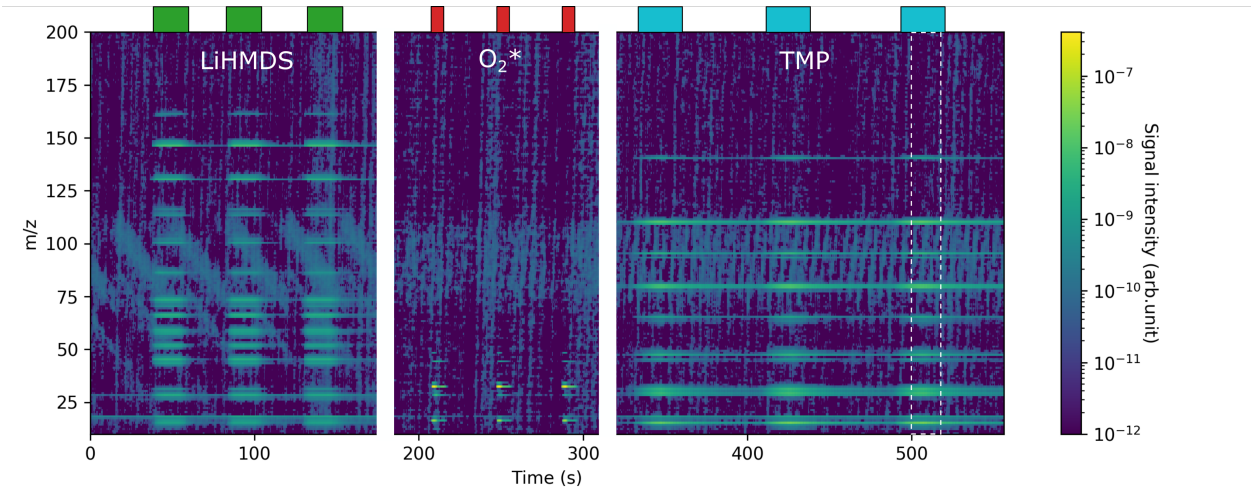

Figure 5: Time-resolved mass spectrum for the LiHMDS-O_2*-TMP process at 300°C. The time-averaged spectrum in the box is shown in Fig. 7 as a reference for TMP. Time-resolved spectra for species of interest during the plasma pulse are shown in Fig. 6. The identification of the peaks can be found in Table 2.

signals that are intrinsic to the oxygen plasma (m/z 16 and 32), and signals from reaction products: peaks for H_2O (m/z 18), CO (m/z 28) and CO_2 (m/z 44), as well as traces of CH_2O (m/z 30) (as proposed in ref[26,27]). The peaks at m/z 34 and 33 could be interpreted as SiH_4 peaks, but they are not transient and have a similar shape to the peaks at m/z 16 and 32, so we interpret them as isotopes of O. The peak at m/z 48 is not transient either and should be interpreted as ozone, probably formed in the in the source of the mass spectrometer as it behaves similarly to the O_2 peaks.

Mass spectrometry during LiHMDS-TMP-O_2*

Once again, little is to be seen during the LiHMDS pulse. In the beginning of the TMP pulse, right before the TMP spectrum itself appears, a reaction product spectrum can be observed similar to the one in Fig. 2. The time-averaged spectrum of this reaction product is again shown in Fig. 7d. The spectra are very similar as can be seen in the vertical cross-sections graphed in Fig. 7c and 7d, although here (Fig. 7d) the intensity of the reaction product is higher. Also at m/z 175 a small peak can be seen now, adding further evidence for the hypothesis that the gaseous reaction by-

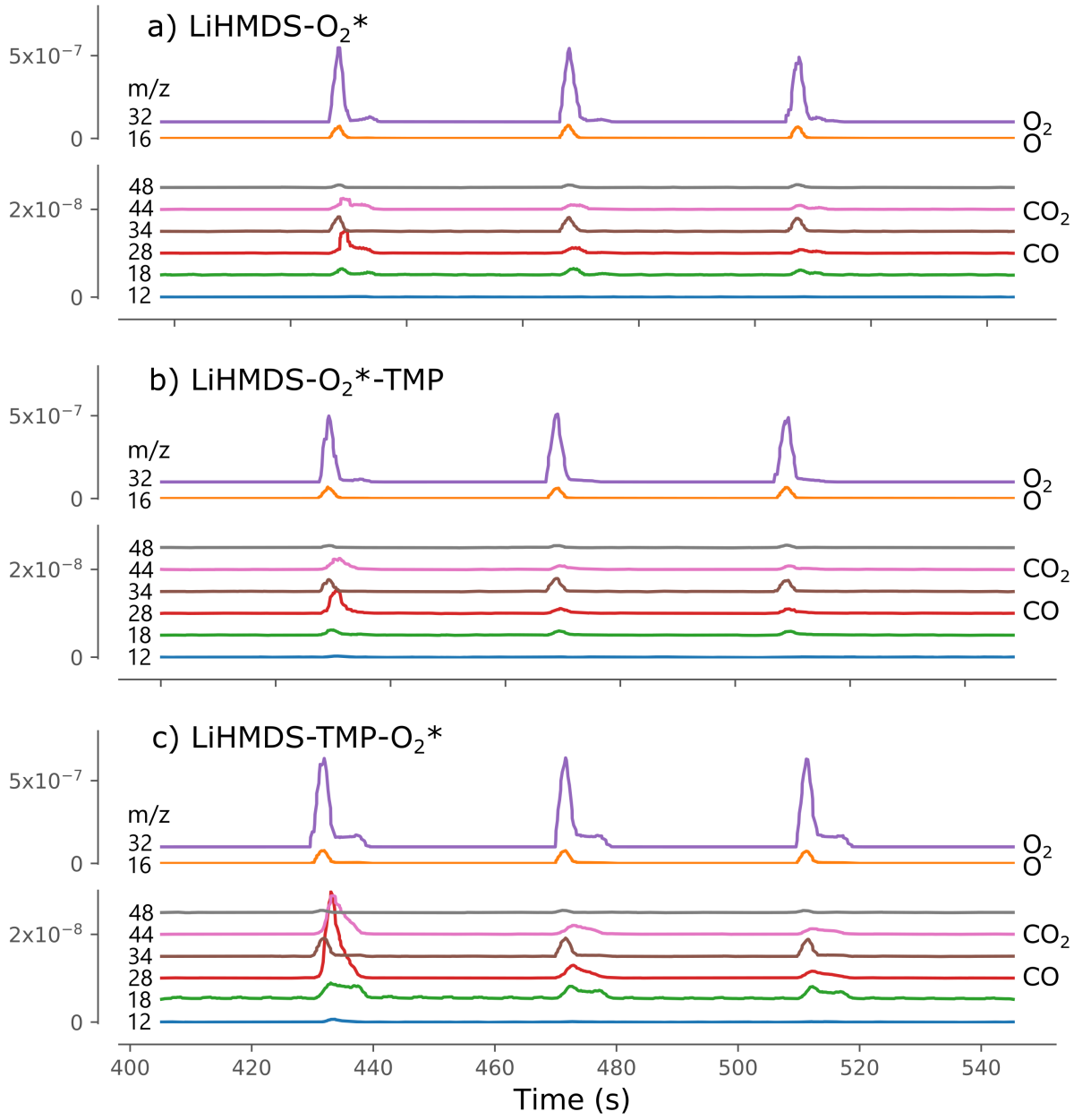

Figure 6: Time-resolved mass spectra of the oxygen plasma pulse during a) LiHMDS-O_2* b) LiHMDS-O_2*-TMP c) LiHMDS-TMP-O_2*. CO_2 (m/z 44, pink) and CO (m/z 28, red) are the main reaction products. It is noteworthy that the signal intensity of the reaction products is higher when the plasma combusts TMP groups, i.e. in case c). The identification of the peaks can be found in Table 2.

product carried away is CH_3HMDS supplemented with lower-mass fragments. The lack of signal at m/z 125 and 155 compared to the TMP pulse in Fig. 2 is another clear difference between the three-step plasma-enhanced process and the LiHMDS-TMP process. During the oxygen pulse, we see similar reaction by-products as in the oxygen pulse in the LiHMDS-O_2* pulse, but the signal intensity almost doubles (see Fig. 6c). This is probably because the preceding TMP pulse leaves the surface in a different state and the surface-plasma reaction is different.

Mass spectrometry during LiHMDS-O_2*-TMP

The most obvious difference between this experiment and the one where the order of TMP and O_2* is reversed is the lack of the reaction product identified as CH_3HMDS when the TMP is pulsed. The oxygen spectrum and the LiHMDS spectrum are very similar to the spectrum in other plasma-enhanced processes. During the LiHMDS pulse, there is a very subtle, minor peak at m/z 160. This might point to the release of CH_3HMDS. LiHMDS has no peak at m/z 160, see Fig. 7, so the peak at m/z 160 may originate from the loss of one of the methyl groups bond to Si. This peak at m/z 160 is shown in Fig. S4. No similar reaction products were found during the LiHMDS pulse in other processes (for example, in Fig. 2). The time averaged spectra during the 3rd TMP pulse are used as reference for TMP in Fig. 7 and Table 2.

Summary

We can summarize the mass spectrometry measurements as follows. When the LiHMDS is followed by TMP, some observable HMDS-like molecule is removed as a reaction product caused by the TMP pulse. It is very likely that this reaction product is CH_3HMDS: the HMDS group from LiHMDS is paired up with a methyl group from the TMP molecule in a ligand-exchange reaction mechanism. A plasma step combusts the remaining surface groups in a typical way creating mainly H_2O, CO and CO_2. However, when the preceding pulse is LiHMDS, the plasma reaction by-products are different compared to when the preceding pulse is TMP. We expect the plasma to leave a mixed hydroxylated and Li-terminated surface. TMP seems not to produce any reaction

products on such a mixed surface, but some P is nevertheless incorporated into the films.

Table 3: Effects of precursors and reactants in different pulsing sequences. All statements except for the CH_3 removal by LiHMDS in LiHMDS-TMP are corroborated by measurements. (s) inferred from film stoichiometry, (g) inferred from growth (m) inferred from mass spectrometry of the pulse itself (m2) inferred from mass spectrometry of the subsequent pulse (m*) inferred from mass spectrometry on another process (x) not observed.

	LiHMDS		TMP		O_2* (Fig. 6)	
LiHMDS-TMP	ligand exchange? (CH_3HMDS) dipole-driven physisorption	(x) (g,m2)	ligand exchange (CH_3HMDS) dipole-driven physisorption	(m) (m2, m*)	n.a.	
LiHMDS-O_2*	dissociative chemisorption dipole-driven physisorption	(s) (g, m*)	n.a.		$Si(CH_3)_3$ combustion LiHMDS combustion	(m,s)
LiHMDS-O_2*-TMP	ligand exchange (CH_3HMDS) dissociative chemisorption dipole-driven physisorption	(m, Fig. S4) (s) (m*)	dipole-driven physisorption	(s)	$Si(CH_3)_3$ combustion LiHMDS combustion	(m,s)
LiHMDS-TMP-O_2*	dissociative chemisorption dipole-driven physisorption	(s) (m2)	ligand exchange (CH_3HMDS) dipole-driven physisorption	(m,g) (s)	$Si(CH_3)_3$ combustion TMP combustion	(m,s)

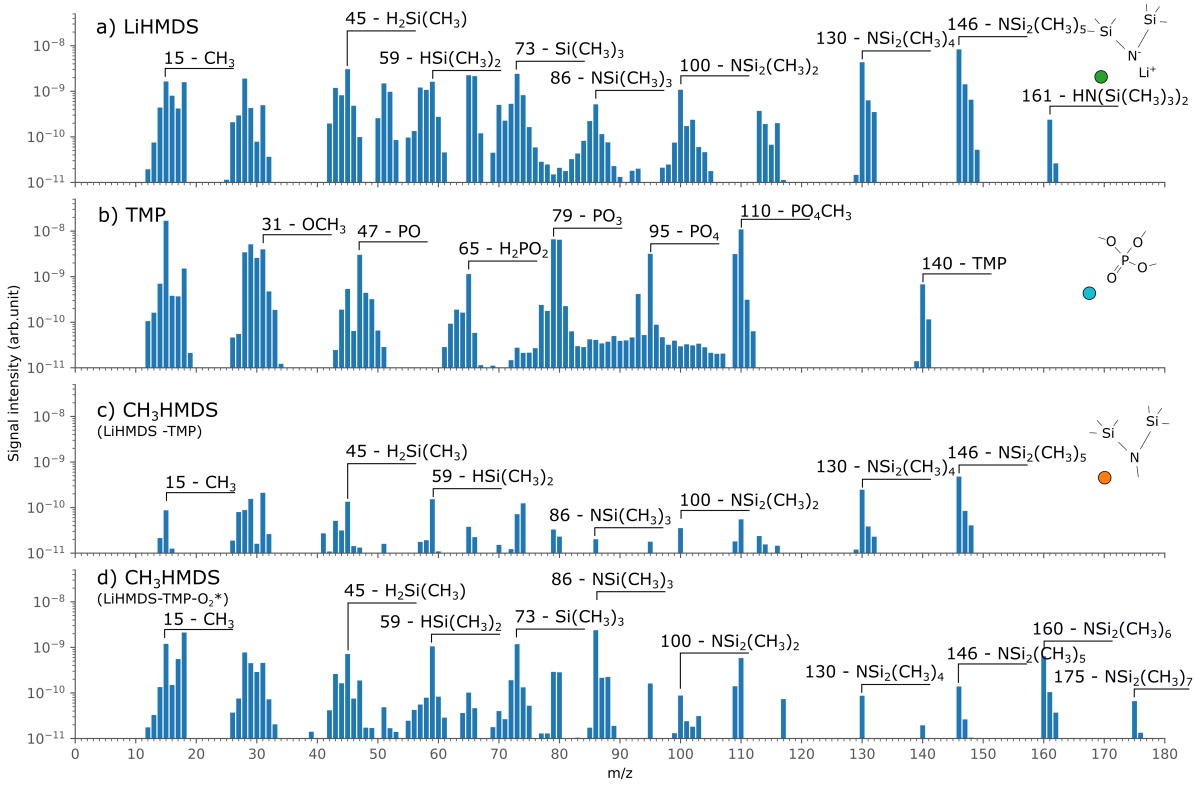

Figure 7: Time averaged spectra at selected times in the different processes. a) The LiHMDS reference was averaged between 130 s and 140 s of the LiHMDS-O_2* process (Fig.3). b) The TMP reference was averaged between 500 s and 520 s of the LiHMDS-O_2*-TMP process (Fig.5). The two CH_3HMDS spectra c) and d) were averaged between respectively 288 s and 291 s for LiHMDS-TMP (Fig.2) and 176 s and 182 s for LiHMDS-TMP-O_2* (Fig.4). The intensity for d) the second CH_3HMDS spectrum is a lot higher, but similar features can be discerned. The CH_3HMDS spectra bear similarity to the LiHMDS spectrum, but are not identical. In both CH_3HMDS spectra there are already some TMP traces visible. The peaks are identified in table 2.

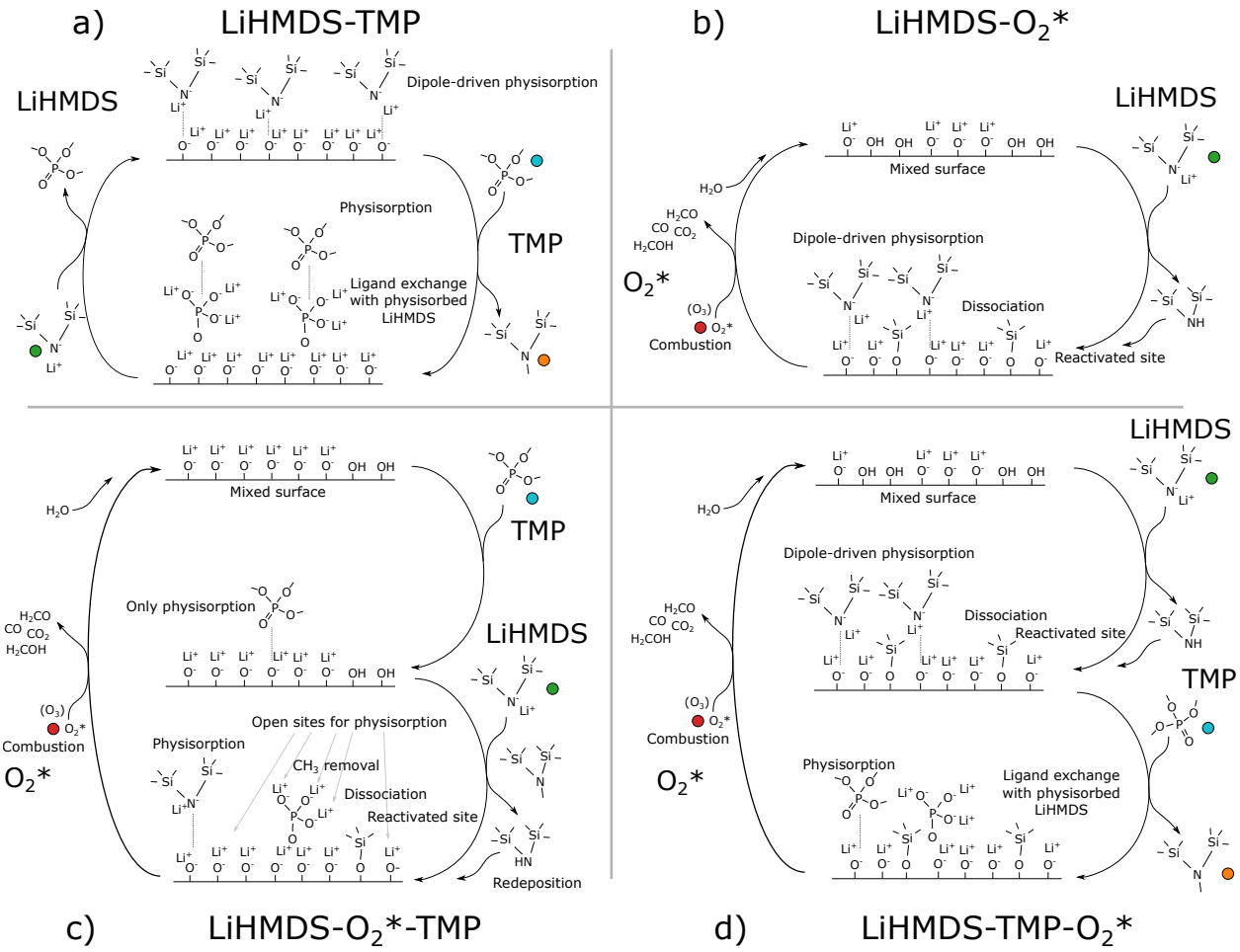

Figure 8: Proposed mechanisms at play in a) the thermal LiHMDS-TMP process without additional oxidizer, which results in a lithium phosphate with the Li_3PO_4 stoichoimetry and b) the LiHMDS-O_2* process, yielding a lithium silicate. c) shows the LiHMDS-O_2*-TMP process and d) the LiHMDS-TMP-O_2* process. Not all reactions are shown completely: the intermediate, reactivated state is indicated as the end state for clarity. As we strived to show all processes, the fractions of molecules may not reflect the actual composition of the samples from Table 1.

Discussion

When considering the measurements presented in the previous section, several interesting questions arise. It is clear that the surface whereupon LiHMDS approaches, is critical for its dual-source behaviour. For both LiHMDS and TMP, we can distinguish between cases where the incoming precursor *reacts* in one or another way with the surface groups, or cases where no reaction product is observed. In that case, it may simply be inert to the surface, or *physisorb*. In the following discussion we will separate the mechanisms that may lead to the incorporation of Li, Si and P in the different films. The occurrence of these mechanisms in the four processes under consideration is assembled in Table 3 and depicted in Fig. 8. They are consistent with the experiments and extend the insights of Tomczak *et al.* [15]

LiHMDS reactions

A first mechanism can be observed when LiHMDS is pulsed in the LiHMDS-TMP process. This process yields Li_3PO_4, hence we expect the surface to consist of O-Li groups. No transient reaction products are observed, so we tentatively assume the precursor physisorbs at the surface:

$$\mathrm{OLi(s)} + \mathrm{LiN(Si(CH_3)_3)_2(g)}$$

$$\longrightarrow \mathrm{OLi|LiN(Si(CH_3)_3)_2(s)} \qquad \text{(C 1)}$$

Lithium is a strongly ionic atom: it tends to donate electrons to surrounding atoms, both in the precursor molecule and in the deposited film. We propose that the driving mechanism for this reaction is the dipole-dipole interaction between the dipole moment created at the surface by the O-Li bond, and the intrinsic dipole moment in the Li-N bond of the precursor. Hence we will use the term *self-saturated dipole-driven physisorption*: the process is self-saturating as the surface dipoles are screened by the adsorbed molecules.

In the LiHMDS-O_2* process which yields lithium silicate, the water produced in the plasma

may generate another surface: a mixed OH/O-Li surface. When the LiHMDS encounters a hydroxyl group instead of an O-Li group, something different happens:

$$\mathrm{OH(s)} + \mathrm{LiN(Si(CH_3)_3)_2(g)}$$

$$\longrightarrow \mathrm{OLi(s)} + \mathrm{HN(Si(CH_3)_3)_2(g)} \qquad \text{(C 2)}$$

The Li atom has replaced the hydrogen at the surface. The HMDS molecule may now compete with the LiHMDS for the remaining OH groups, as described by Tomczak.[15] This leads to Si incorporation.

$$\mathrm{OH(s)} + \mathrm{HN(Si(CH_3)_3)_2(g)}$$

$$\longrightarrow \mathrm{OSi(CH_3)_3(s)} + \mathrm{H_2N(Si(CH_3)_3)(g)} \qquad \text{(C 3)}$$

OH groups at the surface result in dual-source behavior: both silyl groups and lithium can be present at the surface at the end of the LiHMDS pulse via *dissociative chemisorption*[28] of LiHMDS and the redeposition of HMDS. However, we expect the effect of the HMDS to be rather small, as its growth with oxygen plasma is little compared to the LiHMDS-O_2* process (0.039 nm/cycle at 100°Cfor HMDS versus 0.23 nm/cycle at 150°Cfor LiHMDS. See supporting information and Fig. 1.). In the dissociative chemisorption reaction, O-Li surface groups are created. These can trigger in their turn the self-saturated dipole-driven physisorption: the OH-sites are 're-activated' for dipole-driven physisorption in the same precursor pulse. In Fig. 8 this intermediate, reactivated state is indicated as the end state for clarity. The three surface reactions C 1, C 2 and C 3 are occurring at the same time during the LiHMDS pulse on a mixed OH/O-Li surface. However, regardless of the starting surface, at the end of any LiHMDS pulse a blanket of physisorbed LiHMDS molecules will cover the surface.

TMP reactions

When the TMP is pulsed after a LiHMDS pulse, the two precursors meet at the surface. Li from the physisorbed LiHMDS is built into the film, while the HMDS group leaves the surface through the formation of gaseous CH_3HMDS

$$3\text{OLi}|3\text{LiN}(\text{Si}(\text{CH}_3)_3)_2(\text{s}) + \text{O}{=}\text{P}(\text{OCH}_3)_3(\text{g})$$

$$\longrightarrow 3\text{OLi}|\text{Li}_3\text{PO}_4(\text{s}) + 3\text{CH}_3\text{N}(\text{Si}(\text{CH}_3)_3)_2(\text{g}) \qquad \text{(C 4)}$$

Three physisorbed LiHMDS molecules are necessary to fully react the methyl groups of a single TMP molecule. As this may not happen for all molecules, some carbon and hydrogen impurities will be built into the film. However, the major part of the surface now consists again of O-Li groups. We assume the LiPON process of Nisula *et al.*[9] with LiHMDS and diethyl phosphoramidate (DEPA) to behave in a similar fashion.

It is interesting to note that the TMP molecule has a dipole moment as well, and may thus be attracted to the O-Li groups of the newly formed surface, resulting in a similar self-saturating dipole-dipole reaction.

$$\text{OLi(s)} + \text{O}{=}\text{P}(\text{OCH}_3)_3(\text{g})$$

$$\longrightarrow \text{OLi}|\text{O}{=}\text{P}(\text{OCH}_3)_3(\text{s}) \qquad \text{(C 5)}$$

O_2* reactions

When an oxygen plasma pulse reacts with the physisorbed LiHMDS, all methyl groups are combusted, leading to very little contamination compared to the thermal process. The result of the plasma is that the surface methyl groups are replaced with OH groups,[26] so after a plasma pulse we have a mixed Si-OH/O-Li surface.

Ternary processes

The ternary processes further clarify the proposed mechanisms: in the LiHMDS-TMP-O_2* process the HMDS ligand of the physisorbed LiHMDS is removed by the TMP according to reaction C 4. This results in a significant decrease of the growth. This removal is very efficient, and hence little additional P is incorporated in the film (a single P atom accounts for six removed Si atoms). However, the Si groups from the dissociative chemisorption of LiHMDS survive at the surface, leading to reduced TMP physisorption. Their methyl ligands are combusted in the subsequent oxygen plasma pulse. The change from physisorbed LiHMDS to physisorbed TMP at the surface explains the different intensities in the combustion mass spectra recorded during the oxygen plasmas showed in Fig. 6.

The LiHMDS-O_2*-TMP process much resembles the LiHMDS-O_2* process, because the physisorbed LiHMDS stays at the surface and is immediately combusted in the subsequent plasma pulse. It has been shown in literature that TMP reacts only very weakly with OH groups.[29] However, the observation of a transient signal at m/z = 160 points towards a third effect in the LiHMDS pulse. When LiHMDS arrives on a surface where TMP is physisorbed, either the TMP is removed completely due to the stronger dipole (explaining the TMP-like traces in the LiHMDS pulse of the LiHMDS-TMP process), or the methyl groups are removed and PO_4 is incorporated. This is also reflected in the composition of the films. A similar, unobserved removal of methyl groups may occur as well in the two-step LiHMDS-TMP process.

Conclusions

By investigating ALD-grown films where LiHMDS is combined with O_2* and TMP in different pulsing sequences, the importance of the surface whereupon the LiHMDS adsorbs is demonstrated. It is clearly shown that the LiHMDS reaction with the surface has two components: a dissociative chemisorption component when OH groups are present and a dipole-driven, self-saturating physisorption component when O-Li groups are present. The former is demonstrated in the LiHMDS-

TMP-O_2* process, the latter in the LiHMDS-TMP process.

Dissociation is naturally followed by physisorption on newly created O-Li dipoles, and both processes contribute to growth in the LiHMDS-O_2* and the LiHMDS-O_2*-TMP processes. When the surface only consists of O-Li groups, no dissociation will happen and physisorption is the only reaction mechanism.

The subsequent precursor pulse determines the dual- or single-source behavior of LiHMDS: TMP is capable of removing the HMDS component in CH_3HMDS form, so only Li remains at the surface. Oxygen plasma combusts the molecule, leading to the incorporation of Si as well. Combustion leads to a mixed OH/O-Li surface, further enhancing the dual-source behavior via dissociation.

Hence, the single-source behavior of LiHMDS is very specific for processes where a) no hydroxyl groups are present on the pristine surface b) the HMDS ligand of physisorbed LiHMDS is removed in the subsequent pulse. On the other hand, if one of the two conditions is violated, dual-source behavior will emerge and silicon will be incorporated in the deposited films.

We hope that these insights are relevant if LiHMDS is considered for the deposition of lithium-containing films, especially in ternary and quaternary processes.

Acknowledgement

Andreas Werbrouck thanks the Fund for Scientific Research - Flanders (FWO) for a scholarship through an SB grant (number 1S12319N). Hiden Analytical is acknowledged for technical support. The technical help, excellent guidance and useful comments of Thomas Dobbelaere in the initial stages of research into lithium-containing films in the Cocoon group were greatly appreciated.

Supporting Information Available

Supporting Information is available free of charge.

- Additional information on ellipsometry models used.
- XPS depth profiles
- A time-resolved mass spectrum of the LiHMDS-TMP process at 150°C.
- A horizontal slice of m/z = 45, 59 and 74 during the TMP pulse of the LiHMDS-TMP process.
- A horizontal slice of m/z 160 and 161 during the LiHMDS pulse of the the LiHMDS-O_2*-TMP process, showing a transient peak at m/z = 160.
- Saturation curves for HMDS.

References

(1) Nilsen, O.; Gandrud, K. B.; Ruud, A.; Fjellvåg, H. In *Atomic Layer Deposition in Energy Conversion Applications*; Bachmann, J., Ed.; John Wiley & Sons, 2017; Chapter 6, pp 183–207.

(2) Liu, J.; Sun, X. Elegant design of electrode and electrode/electrolyte interface in lithium-ion batteries by atomic layer deposition. *Nanotechnology* **2014**, *26*, 024001.

(3) Mattelaer, F.; Vereecken, P. M.; Dendooven, J.; Detavernier, C. The influence of ultrathin amorphous ALD alumina and Titania on the rate capability of anatase TiO_2 and $LiMn_2O_4$ Lithium ion battery electrodes. *Advanced Materials Interfaces* **2017**, *4*, 1601237.

(4) Chen, K.-H.; Sanchez, A. J.; Kazyak, E.; Davis, A. L.; Dasgupta, N. P. Synergistic effect of 3D current collectors and ALD surface modification for high coulombic efficiency lithium metal anodes. *Advanced Energy Materials* **2019**, *9*, 1802534.

(5) Moitzheim, S.; Put, B.; Vereecken, P. M. Advances in 3D Thin-Film Li-Ion Batteries. *Advanced Materials Interfaces* **2019**, *6*, 1900805.

(6) Dobbelaere, T.; Mattelaer, F.; Dendooven, J.; Vereecken, P.; Detavernier, C. Plasma-enhanced atomic layer deposition of iron phosphate as a positive electrode for 3D lithium-ion microbatteries. *Chemistry of Materials* **2016**, *28*, 3435–3445.

(7) Mattelaer, F.; Geryl, K.; Rampelberg, G.; Dendooven, J.; Detavernier, C. Amorphous and crystalline vanadium oxides as high-energy and high-power cathodes for three-dimensional thin-film lithium ion batteries. *ACS applied materials & interfaces* **2017**, *9*, 13121–13131.

(8) Liu, J.; Xiao, B.; Banis, M. N.; Li, R.; Sham, T.-K.; Sun, X. Atomic layer deposition of amorphous iron phosphates on carbon nanotubes as cathode materials for lithium-ion batteries. *Electrochimica Acta* **2015**, *162*, 275–281.

(9) Nisula, M.; Shindo, Y.; Koga, H.; Karppinen, M. Atomic layer deposition of lithium phosphorus oxynitride. *Chemistry of Materials* **2015**, *27*, 6987–6993.

(10) Kozen, A. C.; Pearse, A. J.; Lin, C.-F.; Noked, M.; Rubloff, G. W. Atomic layer deposition of the solid electrolyte LiPON. *Chemistry of Materials* **2015**, *27*, 5324–5331.

(11) Kazyak, E.; Chen, K.-H.; Davis, A. L.; Yu, S.; Sanchez, A. J.; Lasso, J.; Bielinski, A. R.; Thompson, T.; Sakamoto, J.; Siegel, D. J. et al. Atomic layer deposition and first principles modeling of glassy Li_3BO_3-Li_2CO_3 electrolytes for solid-state Li metal batteries. *Journal of Materials Chemistry A* **2018**, *6*, 19425–19437.

(12) Kazyak, E.; Chen, K.-H.; Wood, K. N.; Davis, A. L.; Thompson, T.; Bielinski, A. R.; Sanchez, A. J.; Wang, X.; Wang, C.; Sakamoto, J. et al. Atomic layer deposition of the solid electrolyte garnet $Li_7La_3Zr_2O_{12}$. *Chemistry of Materials* **2017**, *29*, 3785–3792.

(13) Put, B.; Mees, M. J.; Hornsveld, N.; Sepulveda, A.; Vereecken, P. M.; Kessels, W.; Creatore, M. Plasma-assisted ALD of LiPO(N) for solid state batteries. *ECS Transactions* **2017**, *75*, 61.

(14) Hämäläinen, J.; Munnik, F.; Hatanpää, T.; Holopainen, J.; Ritala, M.; Leskelä, M. Study of amorphous lithium silicate thin films grown by atomic layer deposition. *Journal of Vacuum Science & Technology A: Vacuum, Surfaces, and Films* **2012**, *30*, 01A106.

(15) Tomczak, Y.; Knapas, K.; Sundberg, M.; Leskelä, M.; Ritala, M. In situ reaction mechanism studies on lithium hexadimethyldisilazide and ozone atomic layer deposition process for lithium silicate. *The Journal of Physical Chemistry C* **2013**, *117*, 14241–14246.

(16) Lindblad, M.; Root, A. *Studies in Surface Science and Catalysis*; Elsevier, 1998; Vol. 118; pp 817–826.

(17) Miikkulainen, V.; Ruud, A.; Østreng, E.; Nilsen, O.; Laitinen, M.; Sajavaara, T.; Fjellvåg, H. Atomic layer deposition of spinel lithium manganese oxide by film-body-controlled lithium incorporation for thin-film lithium-ion batteries. *The Journal of Physical Chemistry C* **2014**, *118*, 1258–1268.

(18) Hämäläinen, J.; Holopainen, J.; Munnik, F.; Hatanpää, T.; Heikkilä, M.; Ritala, M.; Leskelä, M. Lithium phosphate thin films grown by atomic layer deposition. *Journal of The Electrochemical Society* **2012**, *159*, A259.

(19) Liu, J.; Tang, Y.; Xiao, B.; Sham, T.-K.; Li, R.; Sun, X. Atomic layer deposited aluminium phosphate thin films on N-doped CNTs. *RSC advances* **2013**, *3*, 4492–4495.

(20) Putkonen, M.; Sajavaara, T.; Rahkila, P.; Xu, L.; Cheng, S.; Niinistö, L.; Whitlow, H. J. Atomic layer deposition and characterization of biocompatible hydroxyapatite thin films. *Thin Solid Films* **2009**, *517*, 5819–5824.

(21) Gandrud, K. B.; Pettersen, A.; Nilsen, O.; Fjellvåg, H. High-performing iron phosphate for enhanced lithium ion solid state batteries as grown by atomic layer deposition. *Journal of Materials Chemistry A* **2013**, *1*, 9054–9059.

(22) Wiedmann, M. K.; Jackson, D. H.; Pagan-Torres, Y. J.; Cho, E.; Dumesic, J. A.; Kuech, T. F. Atomic layer deposition of titanium phosphate on silica nanoparticles. *Journal of Vacuum Science & Technology A: Vacuum, Surfaces, and Films* **2012**, *30*, 01A134.

(23) Werbrouck, A.; Shirazi, M.; Mattelaer, F.; Elliott, S. D.; Dendooven, J.; Detavernier, C. A Secondary Reaction Pathway for the Alumina Atomic Layer Deposition Process with Trimethylaluminum and Water, Revealed by Full-Range, Time-Resolved In Situ Mass Spectrometry. *The Journal of Physical Chemistry C* **2020**,

(24) Østreng, E.; Sønsteby, H. H.; Øien, S.; Nilsen, O.; Fjellvåg, H. Atomic layer deposition of sodium and potassium oxides: evaluation of precursors and deposition of thin films. *Dalton Transactions* **2014**, *43*, 16666–16672.

(25) Nilsen, O. The reservoir effect and its implications. AVS ALD 2015. 2015.

(26) Fomengia, G. N.; Nolan, M.; Elliott, S. D. First principles mechanistic study of self-limiting oxidative adsorption of remote oxygen plasma during the atomic layer deposition of alumina. *Physical Chemistry Chemical Physics* **2018**, *20*, 22783–22795.

(27) Mione, M.; Engeln, R.; Vandalon, V.; Kessels, W.; Roozeboom, F. Infrared and optical emission spectroscopy study of atmospheric pressure plasma-enhanced spatial ALD of Al_2O_3. *Applied Physics Letters* **2019**, *115*, 083101.

(28) Richey, N. E.; de Paula, C.; Bent, S. F. Understanding chemical and physical mechanisms in atomic layer deposition. *The Journal of Chemical Physics* **2020**, *152*, 040902.

(29) Dobbelaere, T.; Roy, A. K.; Vereecken, P.; Detavernier, C. Atomic layer deposition of aluminum phosphate based on the plasma polymerization of trimethyl phosphate. *Chemistry of Materials* **2014**, *26*, 6863–6871.

Graphical TOC Entry